JTTEE5 8:537-544

Reactive Thermal Spray by High Velocity Ceramic Jet and Characterization of the Coatings

T. Kodama, Y. Ikeda, and H. Tamura

(Submitted 7 October 1998; in revised form 12 May 1999)

A ceramic jet composed of molten particles in an electrothermally exploded powder spray was identified by the flash, soft x-ray radiography technique. The velocity of the leading edge of the jet was estimated to be 900 m/s. The coating obtained by a ceramic jet of titanium diboride consisted of a mixing layer of the substrate material and sprayed ceramics. A coating, which exhibited no pores or cracks, was formed through the dense deposition and solidification of spray droplets. The successive impacts of the droplets caused melting and stirring of the substrate surface to form a mixing layer. Some of these layers were formed due to capillary movement of the molten substrate material into the fractures of coarse ceramic particles. Thermal spray by chemical reaction between titanium and boron nitride particles resulted in a composite coating of TiN and TiB_2. The character of the mixing layer indicated that the depth profiles depended on the substrate material.

Keywords ceramic jet, electrothermal explosion, microstructure, reactive thermal spray, titanium boride, titanium nitride

1. Introduction

Nonoxide refractory ceramics, that is, carbides, borides, and nitrides, with resistance against corrosion and wear and high hardness can be thermal sprayed. Some ceramics with high melting points have been sprayed as cermets by conventional thermal spray methods in order to suppress their oxidation and decomposition and to enhance their interparticle bonding and adhesion (Ref 1-3). However, it seems that the cermet coatings would not exhibit the full abilities of the ceramic under high temperature conditions. The fraction of tungsten-monocarbide phase in WC-Co cermet coatings, for instance, would be decreased by the formation of metal-ceramic composites (Ref 4-6). Thus, a new thermal spray method, which could form coatings of such refractory ceramics without any sintering agents and additives, would be beneficial. The authors have investigated the electrothermal explosions of such ceramic powders to study their application as coatings, that is, the electrothermally exploded powder spray (ELTEPS) process (Ref 7-11). The coatings obtained were characterized as a dense deposit of molten particles with mixing of ceramic and substrate materials (Ref 8, 10, 11). Such material mixing is expected to bring strong adhesion of the coating to the substrate. However, the production mechanism and microstructure of the mixing have not been fully characterized.

T. Kodama, Y. Ikeda, and **H. Tamura,** Department of Materials Science and Engineering, Tokyo Institute of Technology, Nagatsuta 4259, Midori-ku, Yokohama 226-8502, Japan. Contact e-mail: tamura@materia.titech.ac.jp.

The velocity of spray particles is very important to cause strong adhesion of coatings to matrices. The optical observation of ELTEPS by the laser Schlieren method revealed the generation of a gas jet, which should include fine molten particles. Though the leading velocity of the gas jet was found to be 3.0 km/s (Ref 9), the high gas density prevented the direct observation of molten particles by Schlieren methods. Thus, the behavior of the particles has not been established.

The reactive thermal spray method has already been conducted to produce intermetallic-compound coatings through the chemical reaction of nickel and aluminum particles (Ref 12). The representative ceramic coatings, which are chemically reacted, are composites of titanium and titanium nitride, Ti-TiN (Ref 13, 14), and nitrogen-deficient titanium nitride, TiN_{1-x} (Ref 15), through the reaction of solid titanium particles with gaseous nitrogen. Because the as-deposited coating exhibited many pores within lamella, the coating was remelted by laser irradiation and densified under solidification (Ref 15). Thus, the process needed a posttreatment. Considering the capabilities of easy change of molar ratio, melting, and dense deposition of titanium and nitride particles by ELTEPS, a new reactive procedure would be expected to produce titanium nitride coating without posttreatment. If nitrogen could be supplied from solid boron nitride, TiN would be produced together with titanium diboride, TiB_2, through the reaction of titanium particles and BN through the ELTEPS process. Therefore, the TiN might be less deficient in nitrogen due to a solid nitrogen source from BN.

In this article the behavior of ceramic jets composed of molten particles was observed by flash, soft x-ray radiography. The microstructure of coatings with material mixing was characterized by electron probe microscopy. The ceramic coating consisting of TiN and TiB_2 was produced by the ELTEPS process using a powder that was prepared by the mechanical mixing of titanium and boron nitride particles.

2. Experimental Setup

The ceramic powder was charged under argon gas at atmospheric pressure in a container, which was concentrically composed of an inner polyethylene tube of electrical insulation and an outer cylindrical metal jacket. The jacket contained a window for the ejection of the tube contents during the explosion. The powders used were zirconium boride, ZrB_2 (particle size: 3 to 5 μm average, purity: 99.5%), titanium boride, TiB_2 (particle size: 10 μm average or less, purity: 99.5%), and the mechanical mixing of titanium (particle size: 150 μm or less, purity: 99.8%) and hexagonal boron nitride, h-BN (particle size: 10 μm average or less, purity: 99.7%). These powders were packed in the tubes at a relative density of 50%. The container was plugged at both ends with a pair of tungsten electrodes, which were fixed by epoxy resin. Reference 9 shows the schematic cross section of a powder container and the viewing area used for the x-ray radiography.

Figure 1 shows the electrical circuit for the electrothermal explosion of the powders and the signal network. The powder container was placed in a vacuum chamber and held by the electrical contacts connected to the circuit. Thus, high voltage and large current were supplied from a large-capacity condenser to the powder. The ceramic jet consisting of high-pressure gas and molten particles generated by the electrical heating of the powder was ejected from the tube through the jacket window during the electrothermal explosion. The maximum voltage and current applied to the powder were 8.3 kV and 90 kA. The energy supplied to the powder was estimated by measuring the voltage and current (Ref 8). A pair of flash x-ray tubes (Scandiflash, Model 150, Sweden) were used for taking time-sequential shadowgraphs of the ceramic jet. Flash, soft x-rays of 35 ns in pulse width were emitted toward the side of the powder container. A delayed-pulse generator allowed a time difference between x-ray pulses. The generator was synchronized with the current discharge in the powder. This observation system is also shown in Fig. 1. The sprays of ZrB_2 and TiB_2 were conducted under dry air of 6.7×10^3 Pa in the chamber, and the Ti-BN powder was sprayed under nitrogen of 6.7×10^3 Pa. Metal substrates were fixed on a plate holder, which faced the jacket window. Mild steel and aluminum substrates were employed. Each substrate had a top surface of 10×10 mm^2 and a thickness of 2 mm. The top surface had been mirror polished to study high temperature and high velocity effects on the surface. The plate holder was positioned at a standoff distance of 80 mm from the container axis. The micromorphology and constituent elements of the coatings were characterized with a scanning electron microscope (SEM, JEOL Co., Model: JSM-5310, Japan) and an electron probe microanalyzer (EPMA, Shimazu Co., Model: EPMA-1400, Japan), respectively. The crystal structure of the coatings was analyzed using an x-ray diffraction analyzer (XRD, Mac Science, Model: M18XHF, Japan). Vickers microhardness of the coatings was measured with a hardness tester (Akashi Co., Model: MVK-EIII, Japan).

3. Experimental Results and Discussion

3.1 Behavior of Ceramic Jet

X-ray radiography was applied to image the shadows of the ZrB_2 jets, the gas flow of which had been already observed by the previous laser Schlieren method (Ref 9). Figure 2 shows typical electrical waveforms of the explosion. The electrothermal

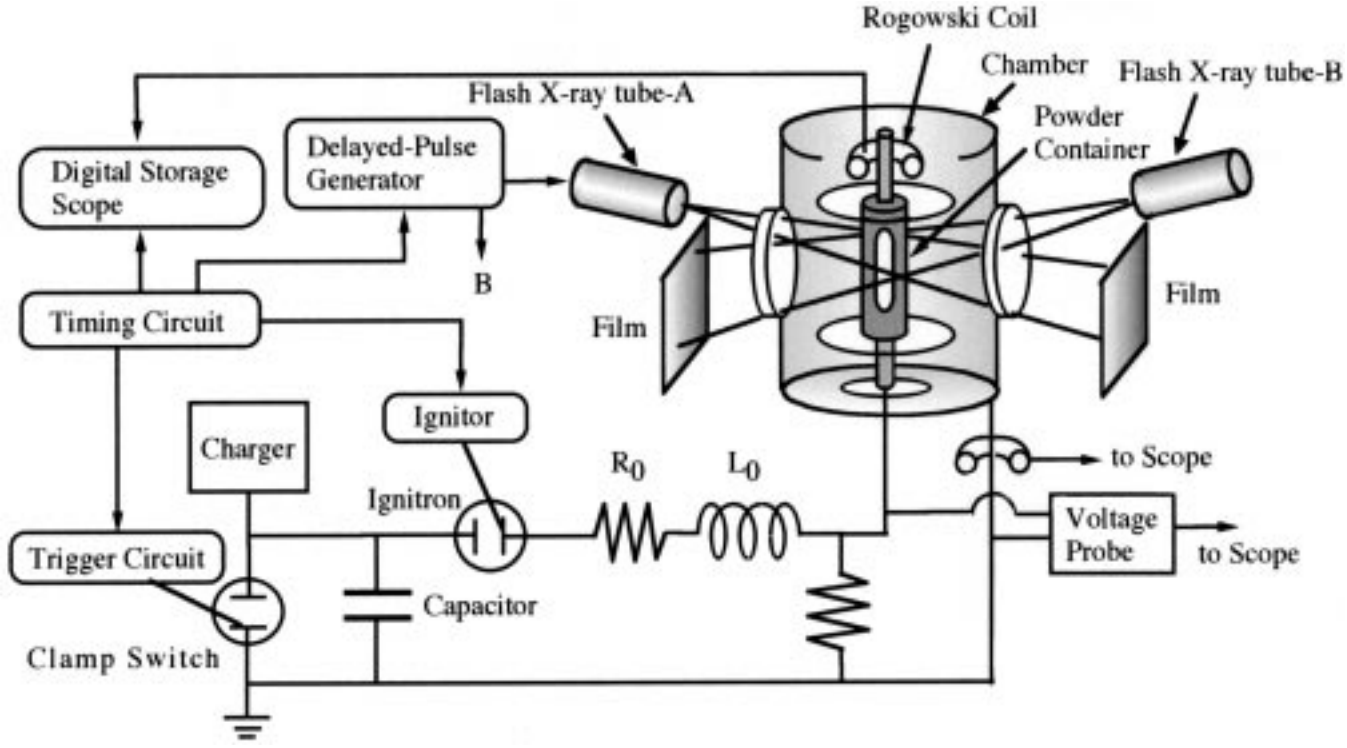

Fig. 1 Experimental setup for electrothermally exploded powder spray

explosion of ceramic powders is characterized by the behavior of the apparent resistance shown in Fig. 2(c). According to prior work (Ref 9), the first exponential decrease of the resistance until 30 μs is due to the heating of argon gas and the enlargement of contact surfaces of the powder particles. The plateau on the curve during 30 and 59 μs corresponds to further heating of the particles with higher resistivity. However, the second rapid decrease, which started at 59 μs marked by arrow β had been considered to be due to either (a) a large ejection of high-resistive powder particles, which leaves low-resistive gas inside the container and/or (b) the formation of another current path outside the powder container. Hence, this decrease has not been precisely identified.

Figure 3 shows the radiographs in time sequence. Figures 3(a) and (d) were taken at different times in the explosion shown in Fig. 2, while another explosion was imaged by Fig. 3(b) and (c). The time shown in each figure originated from the onset of the second decrease. The figure shows faint shadows extending from the powder container standing at the left side to the free space in the right side. Because soft x-rays can be masked easily by solid matter, but not effectively by gas, the shadows obtained indicate the groups of fine particles. According to the resolution of this radiography, individual particles less than 100 μm cannot be imaged sharply. Thus, the shadows observed are images from large groups of the starting particles. Such groups start to jet at several positions in the jacket window and fill it up. Such ceramic jets rarefy under spreading to the free space. The leading

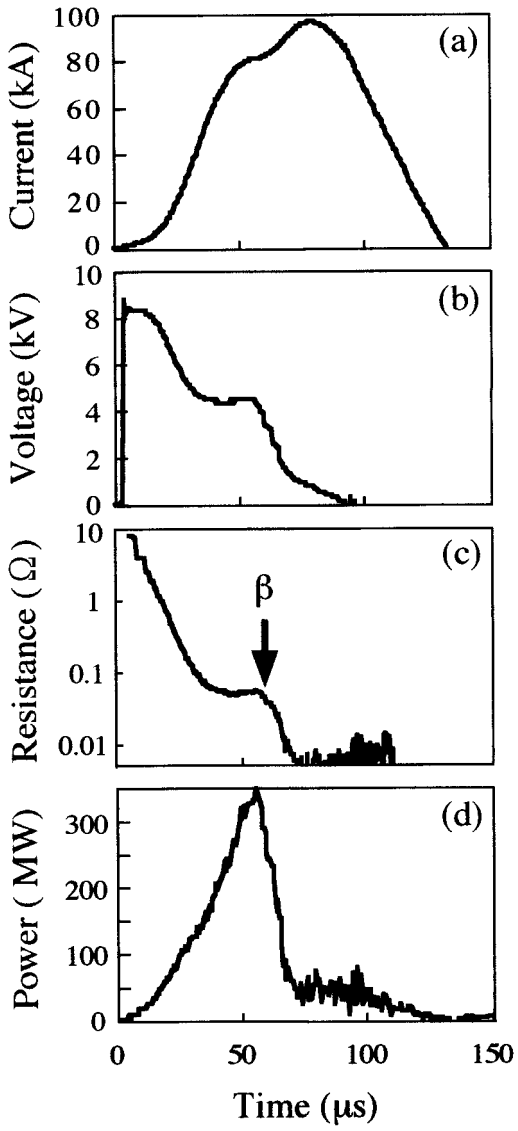

Fig. 2 Electrical characteristics of the explosion of zirconium boride powder. The applied current and voltage are shown as a function of time in (a) and (b), respectively. The apparent resistance of the powder and the electric power supplied are also shown in (c) and (d), respectively.

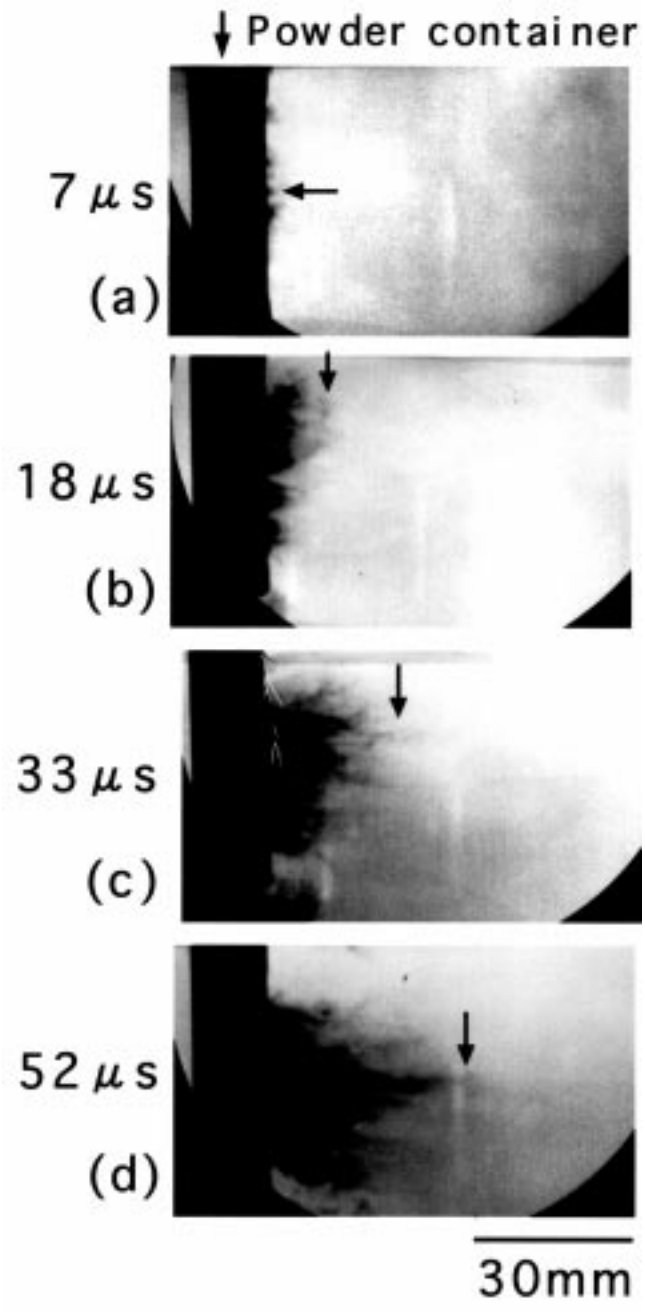

Fig. 3 Soft x-ray shadowgraphs of zirconium boride jets in time sequence. The white thin lines seen by the shadow of the powder container in (c) were exposures of local static electricity on a film.

edges of the shadows are indicated by the arrows. The velocity of the leading edge is estimated to be 900 m/s from two successive shadowgraphs. However, other individual small particles, which would be ahead of the leading edge, might be accelerated to velocities greater than 900 m/s due to gas flow greater than 3.0 km/s (Ref 9). Based on the leading-edge position in the first frame, Fig. 3(a) and the velocity, it is found that the onset of the second decrease of the resistance corresponds to the beginning of the large amount of jetting.

The total electric energy supplied to the powder until the beginning of jetting indicated by the arrow β (Fig. 2c) was estimated to be 10.0 ± 0.7 kJ, while the theoretical energy necessary to melt the ZrB_2 powder was 4.6 kJ (Ref 8). Thus, the powder should be melted. The electric energy was converted to the heating and melting of the powder, the kinetic energy of the molten particles, and the deformation of the container.

3.2 Observation of Microstructure of TiB_2 Coating

Figure 4 shows scanning electron microscopy (SEM) images of the feedstock and a coating surface obtained on a mild-steel substrate. No morphological details of the starting particles can be observed. The energy supplied to the TiB_2 powder was 11.2 kJ, which is approximately three times the theoretical energy to heat the powder up to a melting point of 3190 K (Ref 16) without any losses. Therefore, the molten particles impact the substrate and flatten. The rapid cooling caused some cracks in the coating. The x-ray diffraction (XRD) analysis of the coating surface revealed that there was only two crystal phases of TiB_2 and iron without any due to decomposition and chemical reaction.

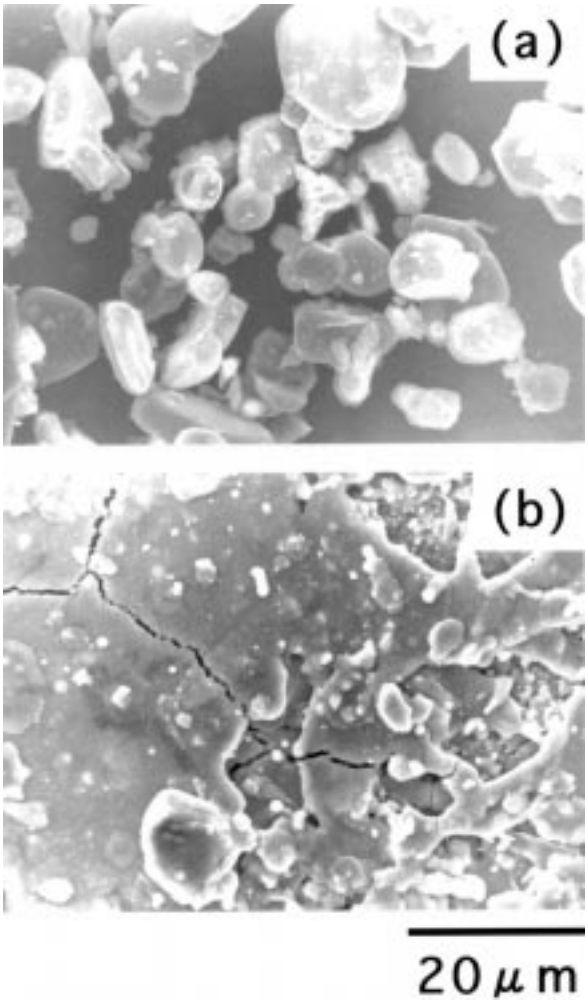

Fig. 4 Scanning electron microscope (SEM) images of (a) starting powder of titanium boride and (b) coating surface obtained on a mild-steel substrate

Figure 5(a) shows a SEM image of the cross section of a TiB_2 coating produced on a mild-steel substrate. The element analyses of titanium and iron on the cross section are shown in Fig. 5(b) and (c), respectively. Each bright area is rich in the analyzed element. The appearance of titanium indicates the existence of TiB_2 according to the XRD analysis, and the iron distribution mapped in Fig. 5(c) shows the mixing of iron with TiB_2. Such mixing ranges 50 μm deep from the coating top surface. No pores or cracks were found in the mixing, while the top surface consisting of only the ceramics had the cracks, as shown in Fig. 4(b). Accordingly, the coating was formed through the dense deposition and solidification of spray droplets. The coatings on an aluminum substrate also exhibited a similar mixing behavior of the materials.

Figure 6 shows the other SEM images of the mixing obtained on a mild-steel substrate. The coarse (several to 10 μm in size) and fine (<1 μm) TiB_2 particles (dark-colored) coexist in the mixing. According to energy-dispersive x-ray (EDX) spectroscopy, the coarse particle marked A was composed of TiB_2 and did not contain iron. The magnification of the area B is shown in Fig. 6(b). Further magnification of the area C is given in Fig. 6(c). The EDX analysis on Fig. 6(c) detected both TiB_2 and iron. The microstructure shown consists of fine TiB_2 particles; the crevices between are filled with iron. In Fig. 6(a) these fine TiB_2 particles profile an imaginary coarse particle, which would be as large as particle A. Considering the good wetting of iron and TiB_2 (Ref 17), and the microstructure, such an imaginary particle was originally coarse, which fragmented under rapid cooling and densified by the capillary action of molten iron. It is also expected that this process occurred in the cross section shown in Fig. 5. A magnification of a square area in Fig. 5(a) is given in Fig. 5(d). The microstructure seen is similar to that in Fig. 6(c). Therefore, a group of fine particles surrounded by an ellipse in Fig. 5(a) appear to have originated from a coarse particle. Such a coarse particle would incorporate a cluster of fine molten particles, which might be produced in the powder container or in the mixing on the substrate.

The formation process of the material mixing is modeled as follows: The starting powder particles are joule heated in the polyethylene tube, and some of them gather into coarse molten particles. Coarse and fine particles spout out during the rupture of the tube, forming a ceramic jet with high temperature and high velocity. The jet deposits due to successive impacts of the particles on the substrate surface. The surface begins to melt due to heat conduction and is stirred violently by the impact of the jet accompanied by shock waves in the substrate. Then the mixing of molten materials occurs. When the mixing area begins to cool, the TiB_2 molten particles solidify faster than iron because the melting point of iron is much lower (by 1300 K) than that of TiB_2. Such cooling might induce the recrystallization of fine particles and the fracture of coarse particles. Because the iron is

still molten, it penetrates cracks between the TiB_2 particles under the fracture.

3.3 Thermal Spray Coating of the Ti-B-N System

The chemical reaction of titanium and boron nitride is expected as:

$$13\,Ti + 10\,BN \rightarrow 5\,TiB_2 + 8\,TiN_{1-x} + (1 + 4x)\,N_2$$

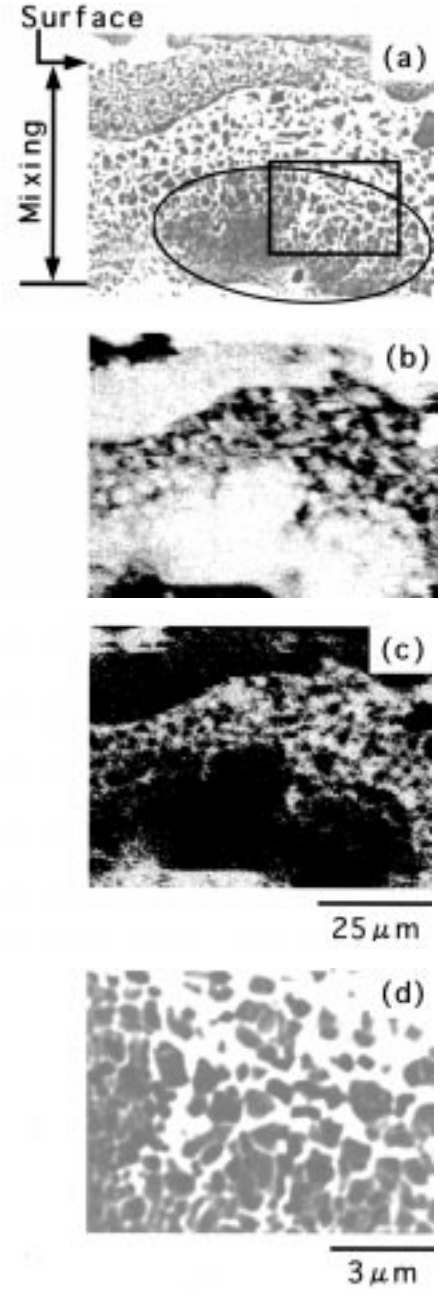

Fig. 5 (a) Scanning electron microscopy image of a cross section of titanium boride coating obtained on a mild-steel substrate. (b) Titanium element map on a mild-steel substrate. Bright area is rich in an analyzed element. (c) Iron element map. (d) Magnification of the area in the square on (a)

This molar ratio of titanium and BN was chosen to allow the mixed powder to have sufficient electric conduction and decrease the nitrogen-deficiency, x in TiN_{1-x}. The joule heat supplied to the Ti-BN powder was 7.9 kJ. The heat of formation for the amount of this system was 1.5 kJ. Thus the total heat was 9.4 kJ.

Figure 7 shows the SEM images of the starting powder particles and a coating surface obtained on a mild-steel substrate. Titanium and BN particles are marked by arrows A and B, respectively. The coating surface shown in Fig. 7(b) does not exhibit any of the morphological features of the feedstock

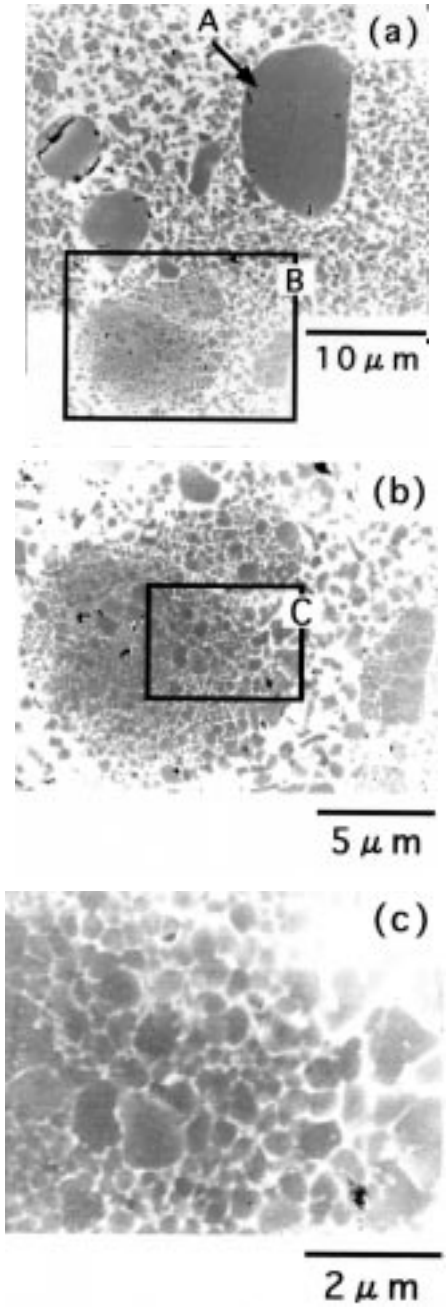

Fig. 6 (a) Scanning electron microscopy image of other cross section of titanium boride coating obtained on a mild-steel substrate. (b) Magnification of the square area B on (a). (c) Magnification of the square area C on (b)

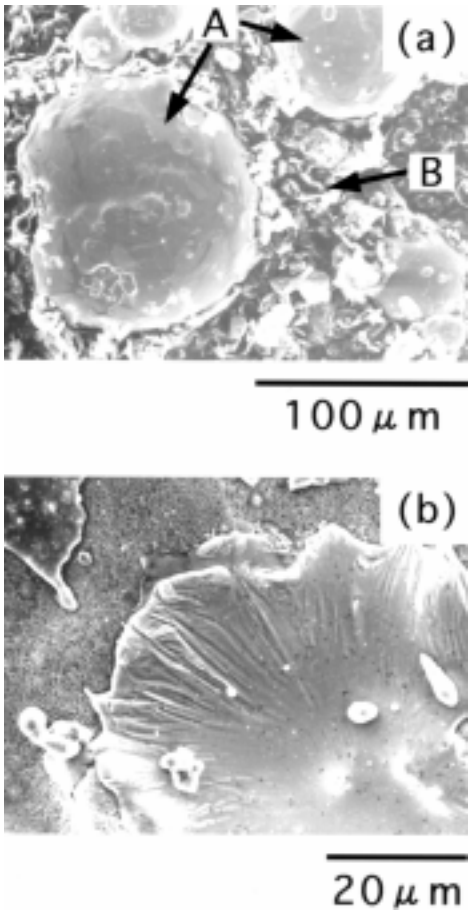

Fig. 7 Scanning electron microscopy images of (a) starting powder composed of titanium A and boron nitride B, and (b) coating surface obtained on a mild-steel substrate

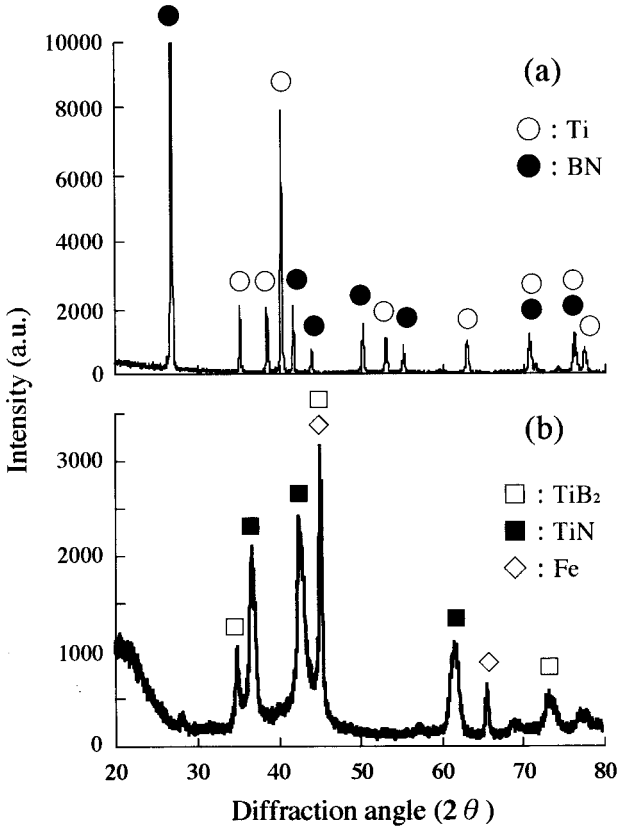

Fig. 8 X-ray diffraction patterns of (a) starting powder composed of titanium and boron nitride, and (b) coating obtained on a mild-steel substrate

particles. The coating was obtained by the flatting and deposition of molten particles on the substrate during the impact.

Figure 8 shows the XRD patterns of the feed stock and the coating surface. The XRD from the coating surface consists of only TiB_2 and TiN, but no titanium, BN, and iron composites. It is found that the composite coating of TiB_2 and TiN was produced by a chemical reaction. Though it was not confirmed where the chemical reaction was caused, it is presumed that most of the mixed-powder particles would react in the polyethylene tube because the particles should be much closer together in the tube than in the jet.

Figure 9(a) shows the SEM image of the cross section of the composite coating produced on a mild-steel substrate. The elemental analyses of titanium and iron on the cross section are shown in Fig. 9(b) and (c), respectively. The appearance of titanium indicates the existence of TiB_2 and TiN according to the XRD analysis, and the iron distribution mapped in Fig. 9(c) shows the mixing of iron with TiB_2 and TiN. This mixing ranges over 30 μm deep from the coating top surface. No pores or cracks are observed in the coating. Accordingly, the coating was formed through the dense deposition and solidification of spray droplets. Figure 9(d) shows the depth profile of iron on the cross section. The region of the sample where detection was employed for the profile is marked in Fig. 9(c). According to the depth profile of iron, the top region to 15 μm deep is occupied mainly by ceramics, while the proportion of the iron constituent increases gradually at 20 μm in depth up to 50% of the iron substrate.

The Vickers microhardness of the mixing layer obtained by five tests ranged from 12.5 to 23.7 GPa (17.8 GPa average), when the load and loading time was 50 gf and 10 s. These are smaller than those of bulk TiB_2 and TiN, that is, 34.4 and 20.9 GPa, respectively (Ref 18). The low experimental values result from the mixing of iron, which has a hardness of 1.4 GPa.

Figure 10 shows the SEM image and element analyses of the cross section of the ceramic coating produced on an aluminum substrate. No pores or cracks were found in the coating. The XRD analysis revealed only the production of TiB_2 and TiN, but no aluminum compounds. Thus, the appearance of titanium in Fig. 10(b) corresponds to the existence of TiB_2 and TiN. The comparison of these element maps shows that the material mixing range is 40 μm. The depth profile of aluminum on the cross section is shown in Fig. 10(d). It is seen that aluminum exists predominantly after a few micrometers from the top surface and that the relative proportion of the aluminum is 75% of the aluminum substrate over the mixing layer.

The Vickers microhardness of the mixing layer was approximately 1.36 GPa. This resulted from the small hardness, 0.39 GPa, of aluminum and the heavy mixing.

Considering that the melting point and density of aluminum are much smaller than those of iron, it is feasible that the aluminum would be mixed easier with the sprayed ceramics than the corresponding behavior of an iron substrate.

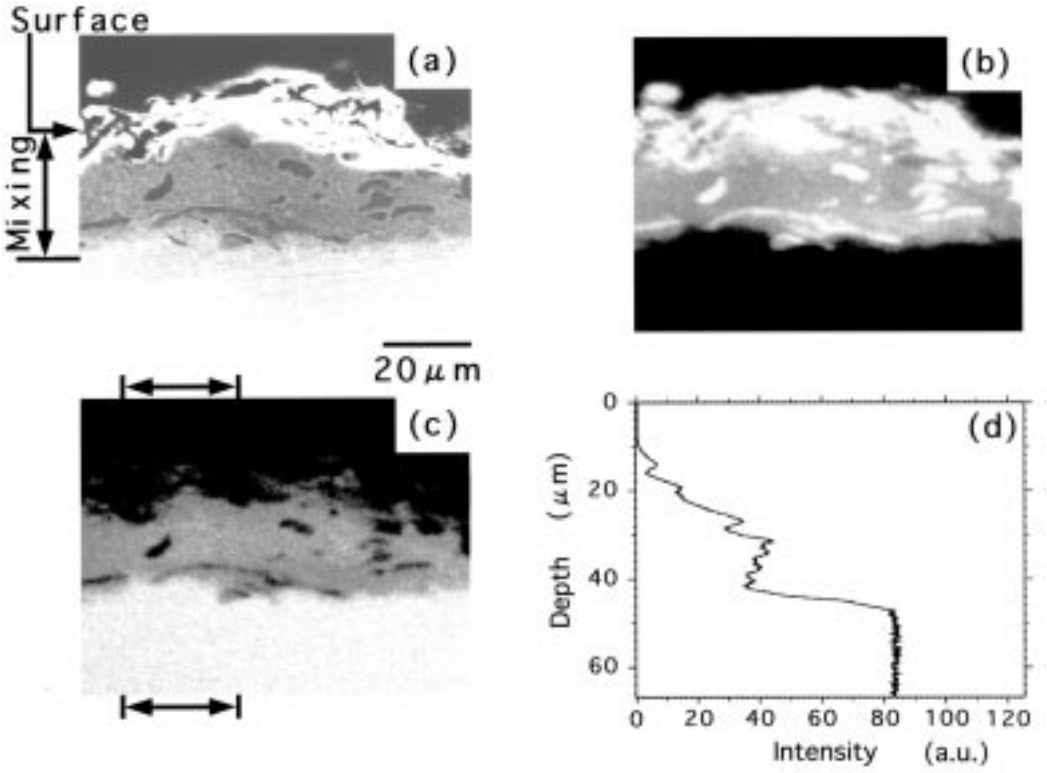

Fig. 9 (a) Scanning electron microscopy image of a cross section of composite coating of titanium boride and titanium nitride obtained on a mild-steel substrate. (b) Titanium element map on a mild-steel substrate. Bright area is rich in an analyzed element. (c) Iron element map. (d) Depth profile of iron in a local area marked by the arrow on (c)

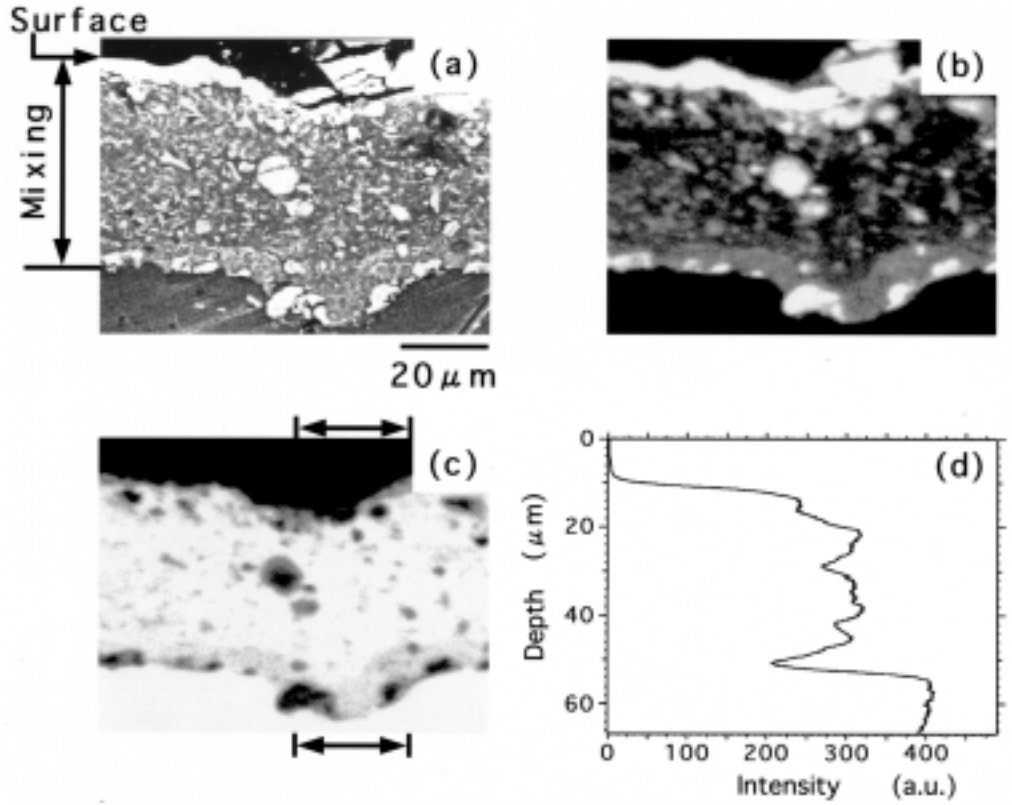

Fig. 10 (a) Scanning electron microscopy image of a cross section of composite coating of titanium boride and titanium nitride obtained on an aluminum substrate. (b) Titanium element map on an aluminum substrate. Bright area is rich in an analyzed element. (c) Aluminum element map. (d) Depth profile of aluminum in a local area marked by the arrow on (c)

The reactive thermal spray is modeled as follows: The conductive titanium particles are heated preferentially during the electric discharge in the polyethylene tube. The BN particles are heated due to thermal conduction from the titanium. The 7.9 kJ heat of the powder is larger than the free energy of activation of the BN particles, which is estimated to be 1.9 kJ. Thus, the activated BN should react with the titanium, followed by the production of titanium boride and nitride.

4. Conclusions

The following conclusions can be drawn:

- The behavior of powder particles in the ELTEPS process was revealed by flash, soft x-ray radiography. The powder particles and argon gas in the tube were joule heated by a large current from the condenser. When the electric energy was supplied sufficiently to heat and accelerate the powder, the powder tube was ruptured, and the high-velocity ceramic jet consisting of the molten particles was generated following the gas ejection.
- The microstructure of the mixing layer consisted of the sprayed material and substrate, and its production mechanism was characterized by the invasion of the molten substrate material into the fracture of coarse ceramic particles through capillary action and by the recrystallization of fine ceramic particles.
- The reactive thermal spray coating composed of TiN and TiB_2 was produced by ELTEPS using a mixed powder of titanium and boron nitride. It was confirmed that the depth profile of the mixing layer depended on the substrate material.

Acknowledgments

This work was supported by Grants in Aid for Exploratory Research 09875175 and Scientific Research (B) 08555169 of the Ministry of Education, Science, Sports, and Culture in Japan. The authors would like to thank Japan New Metals Co., Ltd., Sumitomo Sitix Co., and Shin-Etsu Chemical Co., Ltd., for supplying zirconium boride, titanium, and boron nitride, respectively.

References

1. S. Dallaire and G. Cliche, Tribological Properties of TiC-Fe Coatings Obtained by Plasma Spraying Reactive Powders, *J. Therm. Spray Technol.*, Vol 2, 1993, p 39-44
2. H.J. Kim, Y.G. Kweon, and R.W. Chang, Wear and Erosion Behavior of Plasma-Sprayed WC-Co Coatings, *J. Therm. Spray Technol.*, Vol 3, 1994, p 169-178
3. S. Sampath and S.F. Wayne, Microstructure and Properties of Plasma-Sprayed Mo-Mo_2C Composites, *J. Therm. Spray Technol.*, Vol 3, 1994, p 282-288
4. J. Nerz, B. Kushner, and A. Rotolico, Microstructural Evaluation of Tungsten Carbide-Cobalt Coatings, *J. Therm. Spray Technol.*, Vol 1, 1992, p 147-152
5. H.S. Ahn, and C.H. Lee, A Study on the Wear Characteristics of Plasma Sprayed NiCrSiB/WC-12Co Mixed Coating, *Thermal Spray: Meeting the Challenges of the 21st Century*, Vol 1, C. Coddet, Ed., ASM International, Vol 1, 1998, p 175-180
6. T. Akasawa and K. Ai, Wear Properties of WC/Co Coatings with Plasma and High Velocity Oxyfuel Spraying, *Thermal Spray: Meeting the Challenges of the 21st Century*, Vol 1, C. Coddet, Ed., ASM International, 1998, p 281-286
7. H. Tamura, M. Nagahama, Y. Tanabe, and A.B. Sawaoka, Spraying of Zirconium-Diboride Powder by an Electrical Column Explosion Technique and its Mechanism, *J. Appl. Phys.*, Vol 75, 1994, p 4695-4703
8. H. Tamura, M. Konoue, and A.B. Sawaoka, Zirconium Boride and Tantalum Carbide Coatings Sprayed by Electrothermal Explosion of Powders, *J. Therm. Spray Technol.*, Vol 6, 1997, p 463-468
9. H. Tamura, M. Konoue, Y. Ikeda, T. Soda, and A.B. Sawaoka, Generation of a High-Velocity Jet in the Electrothermal Explosion of Conductive Ceramic Powders, *J. Therm. Spray Technol.*, Vol 7, 1998, p 87-92
10. Y. Ikeda, H. Tamura, and A.B. Sawaoka, Refractory Boride and Nitride Ceramic Coatings Sprayed by Ceramic Jets, *Proc. Int. Conf. AIRAPT-16 and HPCJ-38*, Vol 7, 1998, p 1472-1474
11. T. Soda, H. Tamura, and A.B. Sawaoka, Refractory Carbide Coatings Sprayed by Electrothermal Explosion of Conductive-Ceramic Powders, *Thermal Spray: Meeting the Challenges of the 21st Century*, Vol 2, C. Coddet, Ed., ASM International, 1998, p 1351-1356
12. S. Sampath, B. Gudmundsson, R. Tiwari, and H. Herman, Plasma Spray Consolidation of Ni-Al Intermetallics, *Thermal Spray Research and Applications*, T.F. Bernecki, Ed., ASM International, 1991, p 357-361
13. N. Asahi and Y. Kojima, A Study of Metallurgical Characteristics of Low Pressure Plasma Sprayed Titanium Coatings, *Proc. 7th Int. Conf. Vacuum Metallurgy*, 1982, p 305-312
14. A. Omori, Y.C. Zhang, and Y. Arata, Study on the Reaction Spray of Laser-Plasma Jet-Synthesis of TiN Coatings, *Thermal Spray Research and Applications*, T.F. Bernecki, Ed., ASM International, 1991, p 605-610
15. M. Nishida, E. Maitani, K. Wakatake, T. Araki, Y. Hayashi, and M. Enomoto et al., Densification of Ti-N Laser Sprayed Coatings by Laser Remelting, *J. High Temp. Soc.*, Vol 21, Supplement, 1995, p 265-272 (in Japanese)
16. *High Refractory Elements and Compounds*, R.B. Kontel'nikov, S.N. Basl'ikov, Z.G. Galiakbarov, and A.I. Kastanov, Ed., Nissotsuushinnsha, 1977, p 28 (in Japanese)
17. V.D. Oreshkin, V.I. Svetlopolyanskii, A.D. Panasyuk, and M.S. Borovikova, Investigation of the Interaction of Protective Welding Boride Coatings with Liquid Ferrous Alloys, *Protection of Metals*, Vol 11, 1975, p 219-221
18. *Handbook of Refractory Compounds*, G.V. Samsonov and I.M. Vinitskii, Ed., IFI/Plenum, 1980, p 292, 295